Korean J. Chem. Eng., 38(6), 1188-1196 (2021)
DOI: 10.1007/s11814-021-0778-4

pISSN: 0256-1115
eISSN: 1975-7220

CO_2 hydrogenation activity of Ni-Mg-Al_2O_3 catalysts: Reaction behavior on $NiAl_2O_4$ and $MgAl_2O_4$

Byung Chan Kwon*, No-Kuk Park*,†, Misook Kang, Dohyung Kang*,†, Myung Won Seo***, Doyeon Lee***, Sang Goo Jeon***, and Ho-Jung Ryu*****

*School of Chemical Engineering, Yeungnam University, 280 Daehak-ro, Gyeongsan 38541, Korea
**Department of Chemistry, College of Natural Sciences, Yeungnam University, 280 Daehak-ro, Gyeongsan 38541, Korea
***Korea Institute of Energy Research, Daejeon 34129, Korea
(*Received 23 November 2020 • Revised 8 February 2021 • Accepted 7 March 2021*)

Abstract−CO_2 hydrogenation activity of nickel-magnesium-aluminum mixed oxide catalysts was investigated. As Ni concentration increased, CO_2 conversion increased due to the increased active metal content and suppression of $NiAl_2O_4$ formation. Calcination temperature was found to affect the textural properties of catalysts and to decrease surface area and pore volume significantly. Therefore, catalysts calcined at a relatively low temperature showed high activity, while the particle strength slightly decreased with the reduced calcination temperature. The catalytic activity of reduced $NiAl_2O_4$ and $MgAl_2O_4$ spinel oxides for the hydrogenation of CO_2 was also investigated. $NiAl_2O_4$ dissociated CO_2 to C on reduced Ni, and increased CH_4 selectivity. On the other hand, CO_2 was not fully dissociated, and the CO intermediate was desorbed to produce gaseous CO on reduced $MgAl_2O_4$. Adding MgO suppressed the formation of $NiAl_2O_4$, but CH_4 selectivity decreased due to the formation of $MgAl_2O_4$, indicating the amount of MgO added should be optimized depending on the product required.

Keywords: CO_2 Hydrogenation, CO_2 Methanation, Nickel Aluminate, Magnesium Aluminate, CO Dissociation

INTRODUCTION

Due to increasing carbon dioxide (CO_2) emissions, the global energy paradigm is changing from fossil fuels to renewable energy resources [1,2]. By utilizing environmentally friendly energy sources, the amount of CO_2 emitted can be reduced to control greenhouse gas levels. In addition, CO_2 produced by fossil-based energy systems needs to be captured and stored to mitigate atmospheric CO_2 levels. If the captured CO_2 can be converted into usable resources, which is referred to as carbon capture and utilization (CCU) technology, at reasonable cost, it could be used to reduce atmospheric CO_2 [3-5].

Renewable energies, such as solar and wind power, are intermittent and incompatible with continuous energy production. Therefore, many studies have examined the possibility of storing energy generated using these techniques as chemical energy [6,7]. If minimizing CO_2 is a priority, intermittent renewable energy can be utilized to produce liquefied hydrogen by electrolysis. However, due to high energy cost and technical difficulty associated with liquefying hydrogen, no such system has been commercialized. The use of widely available LNG infrastructure for storing renewable energy as synthetic natural gas (SNG) would provide a near-term solution and prepare society for the introduction of liquefied hydrogen [8,9].

Regarding the storage of renewable energy and CCU, CO_2 could be hydrogenated to produce SNG using renewable energy resources. To be specific, CO_2 emitted from fossil fuel might be captured and reacted with hydrogen produced from the electrolysis of water using renewable energy and SNG could be produced by reacting CO_2 and H_2. SNG could make a great contribution not only as a fuel for transportation and industrial purposes, but also for large-scale energy storage as it is easier to liquify than H_2 [10,11]. Moreover, the carbon monoxide (CO) produced as a by-product of CO_2 hydrogenation could be used as a raw material for liquid petrochemical production using the Fischer-Tropsch (F-T) process [12,13].

Hydrogenation of CO_2 can be divided according to the type of product: CO_2 methanation and the reverse water gas shift (RWGS) reaction. CO_2 methanation was developed to remove CO_2 during the synthesis of ammonia and is currently used to convert CO_2 into CH_4, which suggests its potential use as a power-to-gas (P2G) technology [14]. On the other hand, RWGS is a catalytic conversion technology that produces CO by reacting CO_2 and H_2, which is the reverse of the WGS reaction. RWGS has recently attracted attention as a means of producing CO for the synthesis of methanol, which could be easily stored and used to produce petrochemical products [15,16].

CO_2 methanation: $CO_2+4H_2 \leftrightarrow CH_4+2H_2O$ $\quad \Delta H^o=-164.9$ kJ/mol
RWGS: $CO_2+H_2 \leftrightarrow CO+H_2O$ $\quad \Delta H^o=41.2$ kJ/mol

Catalytic CO_2 hydrogenation proceeds via the Langmuir-Hinshelwood mechanism. After H_2 and CO_2 are adsorbed on metal and metal oxide sites of a catalyst surface, they dissociate to generate adsorbed atomic hydrogen and CO intermediates. The adsorbed CO further dissociates to form atomic carbon intermediates on the catalytic surface, and CH bond formation between surface-adsorbed atomic hydrogen and carbon results in the formation of CH_4. How-

†To whom correspondence should be addressed.
E-mail: nokukpark@ynu.ac.kr, dkang@ynu.ac.kr

ever, if surface-adsorbed CO is not further dissociated and desorbed into the gas phase, CO is produced instead of CH_4. During the process, atomic oxygen from CO_2 reacts with atomic hydrogen to produce water [17,18]. Accordingly, CH_4 is produced by the hydrogenation of surface-adsorbed carbon generated by the stepwise dissociation of CO_2. Since metal surfaces are generally considered active hydrogenation catalysts, a higher catalyst metal content implies a higher methane formation rate.

Nickel-based catalysts such as Ni/Al_2O_3 and Ni-Mg/Al_2O_3 are commercially used for the hydrogenation of CO_2 to methane [19-23], and the Ni component confers high levels of catalytic activity. In these catalysts, MgO and Al_2O_3 act as promotors that increase catalytic activity and stability.

Al_2O_3 supports with high surface areas are used to increase the number of available Ni active sites on catalyst surfaces, and the MgO promoter prevents sintering of Ni/Al_2O_3 at high temperature. Nevertheless, catalytic activity decreases when spinel crystal structures such as $NiAl_2O_4$ and $MgAl_2O_4$ are formed at high temperature [24,25]. In this study, we investigated the effects of Ni content and calcination temperature on the formation of $NiAl_2O_4$ and $MgAl_2O_4$ in nickel-based catalysts and the effect of calcination temperature on the textural properties of catalysts. In addition, we examined the catalytic activity of spinel structures by measuring the CH_4 and CO selectivity for CO_2 hydrogenation. Based on our observations, we observed the reaction behavior of CO_2 hydrogenation on Ni-Mg-Al mixed oxide catalysts.

EXPERIMENTS

1. Preparation of Catalysts

Nickel-magnesium-alumina catalysts were prepared by co-precipitation. Details of the procedure used are provided in Fig. 1. Briefly, nickel nitrate ($Ni(NO_3)_2 \cdot 6H_2O$), magnesium nitrate ($Mg(NO_3)_2 \cdot 6H_2O$), and aluminum nitrate ($Al(NO_3)_3 \cdot 9H_2O$) were dissolved in deionized water. The stoichiometric amount of nitrate precursors required to achieve the weight concentration shown in Table 1 was used. Ammonium bicarbonate ($(NH_3)HCO_3$) was then added drop-wise to this solution to increase the pH 7 to precipitate solid particles. Solid precipitates were then aged in situ for 12 h to allow crystal growth. The slurry mixture was filtered using a filter press, and the solid resultant was dried at 100 °C overnight.

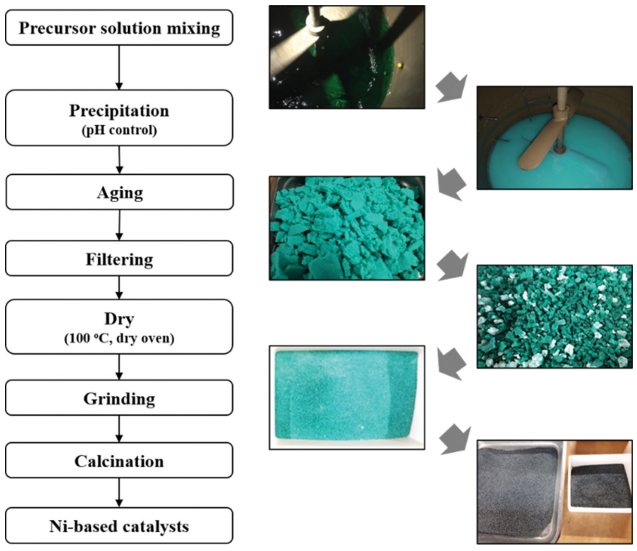

Fig. 1. Catalyst preparation by co-precipitation.

Table 1. Composition of NiO, MgO, and Al_2O_3 in the prepared catalysts

Samples	Composition, wt%		
	NiO	MgO	Al_2O_3
Ni(20)Mg(3)Al(77)	16.6	2.9	80.5
Ni(30)Mg(3)Al(67)	27.5	3.1	69.4
Ni(40)Mg(3)Al(57)	37.7	3.5	58.8
Ni(60)Mg(3)Al(37)	59.3	3.7	37.0

The solid material obtained was then crushed and calcined at 700 °C under air for 4 h. The calcined powder was ground in a ball mill and then DI water was added to form a viscous slurry, which was dried using a spray dryer to produced spherical particles of 150 μm diameter. The catalyst powder was then heat-treated to increase particle strength at 700, 800, 900, and 1,000 °C for 4 h and named Ni(x)Mg(y)Al(100-y), where x, y, and z are metal weight percentages.

To investigate the effect of NiO content on catalytic activity, the amount of NiO was varied from 20 to 60 wt%, while the amount of MgO was fixed at 3 wt% throughout the study. Table 1 shows concentration of NiO, MgO, and Al_2O_3 in prepared catalysts, as determined by ICP-MS at an accuracy of >90%.

$NiAl_2O_4$ and $MgAl_2O_4$ catalysts were prepared with the same procedure above except the amount of the precursors used to examine their abilities to catalyze the hydrogenation of CO_2. In addition, the CH_4 and CO selectivity of prepared catalysts containing different levels of MgO were analyzed. MgO content was varied from 20 to 40 wt%, and NiO content was fixed at 40 wt%.

2. Experimental Setup used to Determine Catalytic Activity

A schematic of the experimental setup is shown in Fig. 2. A fixed

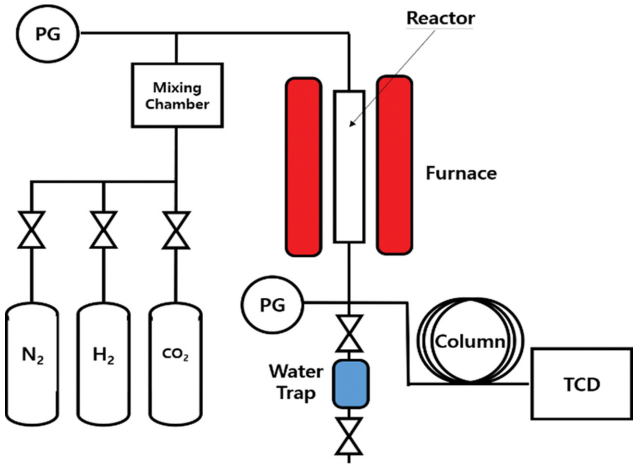

Fig. 2. Schematic diagram of the apparatus used for CO_2 hydrogenation.

bed reactor was used to investigate the catalytic effect of prepared catalysts on CO_2 hydrogenation. Catalyst (1.0 g) was packed inside a tubular (i.d., 1/2 inch) stainless steel (SUS-316) fixed bed reactor, which was heated using a vertical 3-zone furnace. Flow rate of H_2, CO_2, and N_2 was controlled using a mass flow controller (MFC) and passed through a mixing chamber before reaching the reactor.

Before conducting CO_2 hydrogenation, synthesized catalysts were reduced in a nitrogen/10 vol% H_2 mix for 1 h at 500 °C. The reactant mixture (H_2 and CO_2, molar ratio of H_2 to CO_2=4) was then passed into the top of the reactor. Products were condensed out by a water trap installed at the column outlet. After removing of liquid products, dried products were analyzed using a gas chromatograph equipped with a thermo conductivity detector. The mix ratio of H_2 to CO_2 was maintained at 4, which corresponded to the stoichiometric mix required for CO_2 methanation. The flow rate of the reactants was fixed at 500 mL/min, and the calculated space velocity was 20,000-30,000 h^{-1}.

3. Characterization of Catalysts

The composition of catalysts produced by coprecipitation was analyzed ICP-MS (ICP-AES, OPTMA8300, Perkin Elmer, USA), and their crystalline structure was determined by a powder X-ray diffraction (XRD, nickel-filtered CuKα radiation, 40.0 kV and 15.0 mA, Miniflex, Rigaku, Japan). Temperature programmed reduction by H_2 (H_2-TPR) was conducted using BELCAT-B equipped with a thermal conductivity detector. 50 mg of the catalyst was heated to 900 °C at 10 °C/min while flowing a Ar/10 vol% H_2 mix.

Textural properties such as surface area, pore volume, and pore size were determined by isothermal N_2 adsorption-desorption at 77 K (Belsorp II mini, BEL, Japan Inc). Before conducting BET measurements, samples were degassed at 250 °C for 24 h. Attrition testing was conducted according to ASTM-D-5757-95. To measure attrition resistance of the sample particle, a 3-hole chamber which was simulating a fluidized bed system was filled with ~50 g of catalyst powder, and N_2 gas was introduced through 3-hole at 10 L/min to fluidize catalyst powders. The loss of particles caused by friction between particles or against reactor wall was collected on the top of the chamber. Attrition testing was carried out for 5 h, and amount of catalyst lost was measured at 1 h intervals.

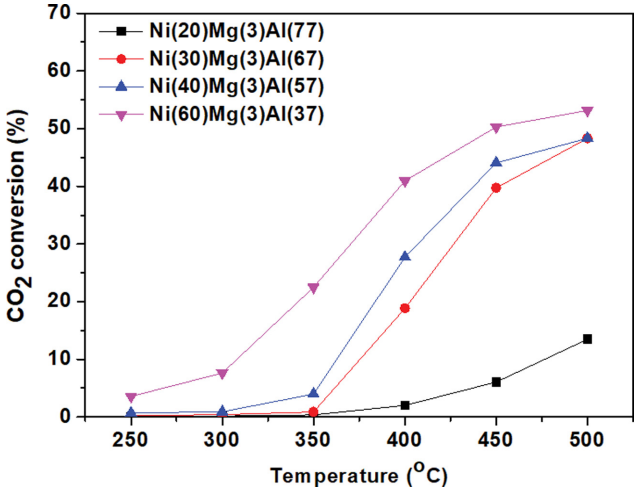

Fig. 3. Conversion of CO_2 over Ni-based catalysts with different NiO content (GHSV=~30,000 h^{-1}).

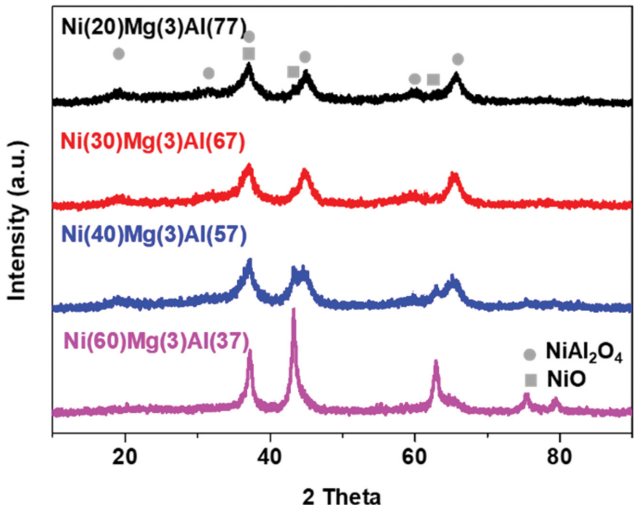

Fig. 4. XRD peak patterns of catalysts with different NiO content (calcination temperature=700 °C).

RESULTS AND DISCUSSION

1. Catalytic Activities at Different Ni Loadings

CO_2 hydrogenation experiments were carried out on the prepared Ni-Mg-Al catalysts containing various amounts of NiO (20 to 60 wt%). The H_2/CO_2 molar ratio was set to 4.0, the volume of catalyst used was 1-1.5 mL, and the flow rate of the nitrogen-diluted reactant (H_2 and CO_2 mixture) was 500 mL/min, which represented a space velocity (GHSV) of 20,000-30,000 h^{-1}.

When the space velocity of CO_2 methanation was relatively low, the exothermic reaction formed a hot-spot in the packed catalyst [26]. In this situation, all catalysts had similar conversion corresponding to the equilibrium value, and it was not possible to compare reaction rates. Therefore, a space velocity of 20,000-30,000 h^{-1} was used to minimize hot-spot formation. When the space velocity of the incoming N_2 diluted reactant mixture was high, the sudden increase in catalyst temperature was suppressed, which allowed reaction kinetics to be easily measured and compared.

CO_2 conversion at temperatures from 250 to 500 °C was measured in terms of different NiO concentrations (Fig. 3). As reaction temperature increased, CO_2 conversion increased for all prepared samples regardless of NiO content. When the activity of catalysts containing different NiO levels was compared at constant temperature (400 °C), CO_2 conversion increased with NiO loading, possibly because of an increase in active Ni in the catalyst. CH_4 selectivity was ~90% for all prepared samples.

Crystalline structures of prepared catalysts with different NiO contents are shown in Fig. 4. The XRD pattern of the $NiAl_2O_4$ spinel structure was mainly observed in Ni(20)Mg(3)Al(77), which also contained a small amount of NiO. The intensity of the NiO pattern gradually increased with NiO concentration, and when this concentration reached 60 wt% in Ni(60)Mg(3)Al(37), the peak pattern of NiO became dominant.

Catalysts calcined at 700 °C were not highly crystalline, but when

the NiO concentration was low (<30 wt%), the $NiAl_2O_4$ spinel structure produced by interaction between NiO and the Al_2O_3 support, was clearly observed. In particular, $NiAl_2O_4$ was a major crystalline phase and NiO a minor phase in Ni(20)Mg(3)Al(77). On the other hand, when catalysts contained a relatively high concentration of NiO (40 wt%), some NiO was transferred to the spinel structure by interacting with Al_2O_3, although most NiO existed as metal oxide. When considering the higher CO_2 conversion with the higher NiO concentration in Fig. 3, the Ni phase which was formed from NiO after H_2 reduction showed higher catalytic activity than the $NiAl_2O_4$ phase. Therefore, many researchers have synthesized catalysts containing excess NiO for the hydrogenation of CO_2 to increase the active Ni phase and to minimize the relatively less active $NiAl_2O_4$ phase. However, NiO optimization in catalysts is essential for commercialization due to the costs involved. In this research, as NiO level >40% substantially increased CO_2 conversion at this level was used in subsequent experiments.

H_2-TPR spectra of Ni(40)Mg(3)Al(67) were obtained in Fig. 5(a) to confirm the reduction characteristics of the catalyst. At a reaction temperature below 500 °C where the CO_2 hydrogenation was conducted, only part of the Ni(40)Mg(3)Al(67) catalyst was reduced. In addition, XRD pattern of the Ni(40)Mg(3)Al(67) catalyst reduced with H_2 at 500 °C showed the presence of strong $NiAl_2O_4$ peaks (Fig. 5(b)), while the intensity of NiO-related peaks decreased significantly compared to the calcined Ni(40)Mg(3)Al(67) (Fig. 4). From these H_2-TPR and XRD results, it can be speculated that the $NiAl_2O_4$ phase was hardly reduced but NiO was possibly reduced into the Ni phase below 500 °C.

2. Effects of Secondary Heat Treatment Temperature on Catalytic Activity

Of the variously sized Ni(40)Mg(3)Al(57) powders prepared using the spray dryer, only particles sized ≥100 μm were subjected to secondary calcination, which was performed to increase particle strength. The particle strength was one of the most important variables to be used for the fluidized bed reactor. The attrition resistance of particles generally increases with calcination temperature-induced density increases, but this could decrease surface area and porosity, and thus, catalytic activity. To investigate the effect of calcination temperature, we varied temperature from 700 to 1,000 °C and maintained heat treatment time at 4 h.

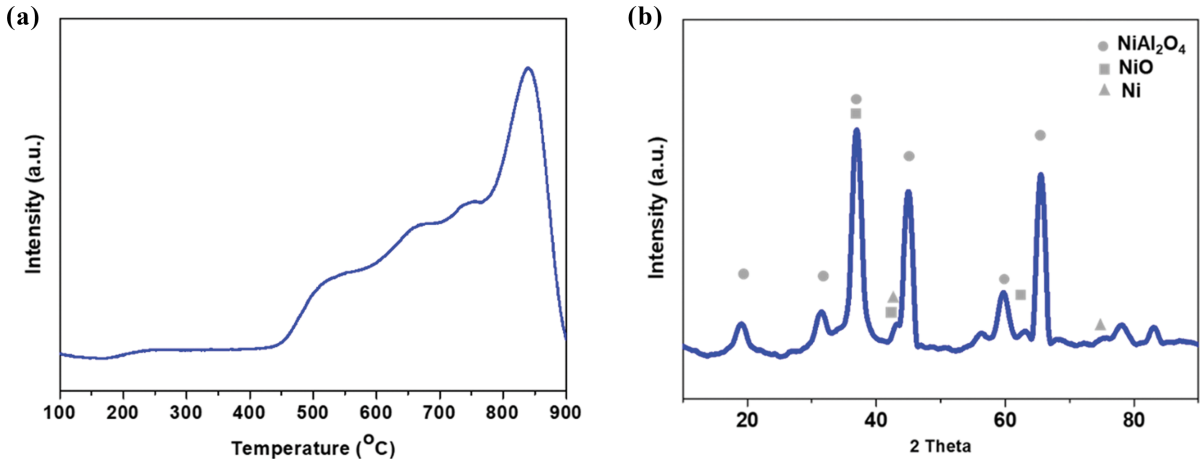

Fig. 5. Reduction characteristics of Ni(40)Mg(3)Al(57); (a) H_2-TPR and (b) XRD pattern of the catalyst reduced at 500 °C.

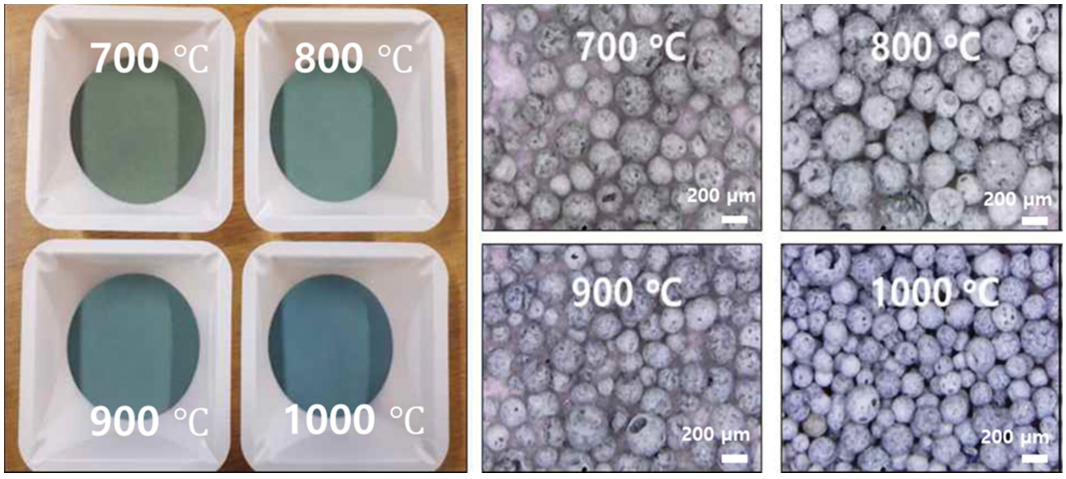

Fig. 6. Optical microscopic image of catalyst particles produced using different calcination temperatures.

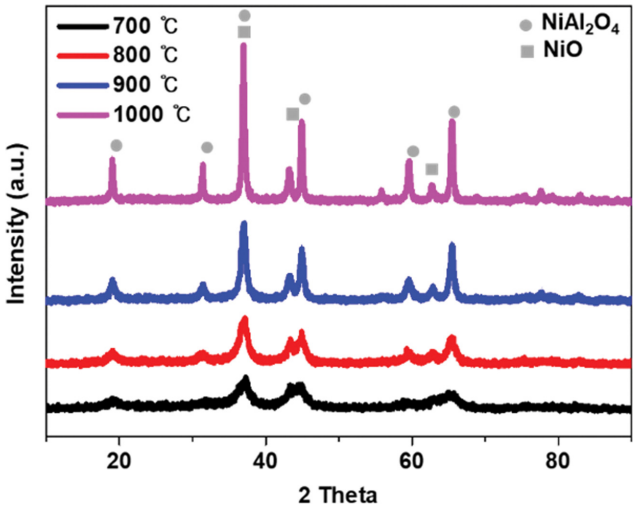

Fig. 7. XRD patterns of Ni(40)Mg(3)Al(57) at different calcination temperatures (700-1,000 °C).

Fig. 6 shows the colors of catalyst powders after calcination. The observed color changes suggested crystallinities had changed. Optical microscopic images also confirmed calcination temperature changed the crystalline structures produced. Furthermore, calcination temperature increases reduced particle sizes, which suggests increases in particle density. When the size of the catalyst particle calcined at different temperatures was compared, the particle size at 700 °C was almost 1.5 times bigger than that calcined at 1,000 °C. Inorganic particle density is generally increased by an amorphous to crystalline phase change. Thus, based on observed changes in powder color and reduction in particle size, it appears that particle crystallinity increased with calcination temperature.

XRD was used to further investigate the crystallinity of particles calcined at different temperatures (Fig. 7). Catalysts calcined at 700 °C showed weak XRD peaks, due to their amorphous content. As calcination temperature was increased, the XRD patterns of NiO and $NiAl_2O_4$ were enhanced. In particular, the relative intensity of $NiAl_2O_4$ to NiO increased with calcination temperature, presumably because NiO interacted more with Al_2O_3 at higher temperature.

As mentioned above, higher catalyst crystallinity generally means lower porosity and surface area. To quantify the surface area and pore volume of Ni(40)Mg(3)Al(57) exposed to different calcination temperatures, N_2 adsorption-desorption isotherms of samples were measured (Fig. 8). Amount of N_2 adsorbed tended to decrease as calcination temperature increased, which also reduced the nitrogen absorbing surface area. In particular, at a calcination temperature of 1,000 °C, the amount of N_2 adsorbed was significantly reduced.

Adsorption/desorption isotherm hysteresis curves provided details about pore morphology and porosity. Hysteresis magnitude decreased as calcination temperature increased, suggesting that porosity also decreased. The specific surface area of catalyst calcined at 700 °C was ~140 m^2/g, which was equivalent to the surface area of gamma alumina calcined at the similar temperature (100-200 m^2/g) (Table 2). However, when the calcination temperature was increased in 100 °C intervals, surface areas decreased to 95, 62, and 23 m^2/g. Pore vol-

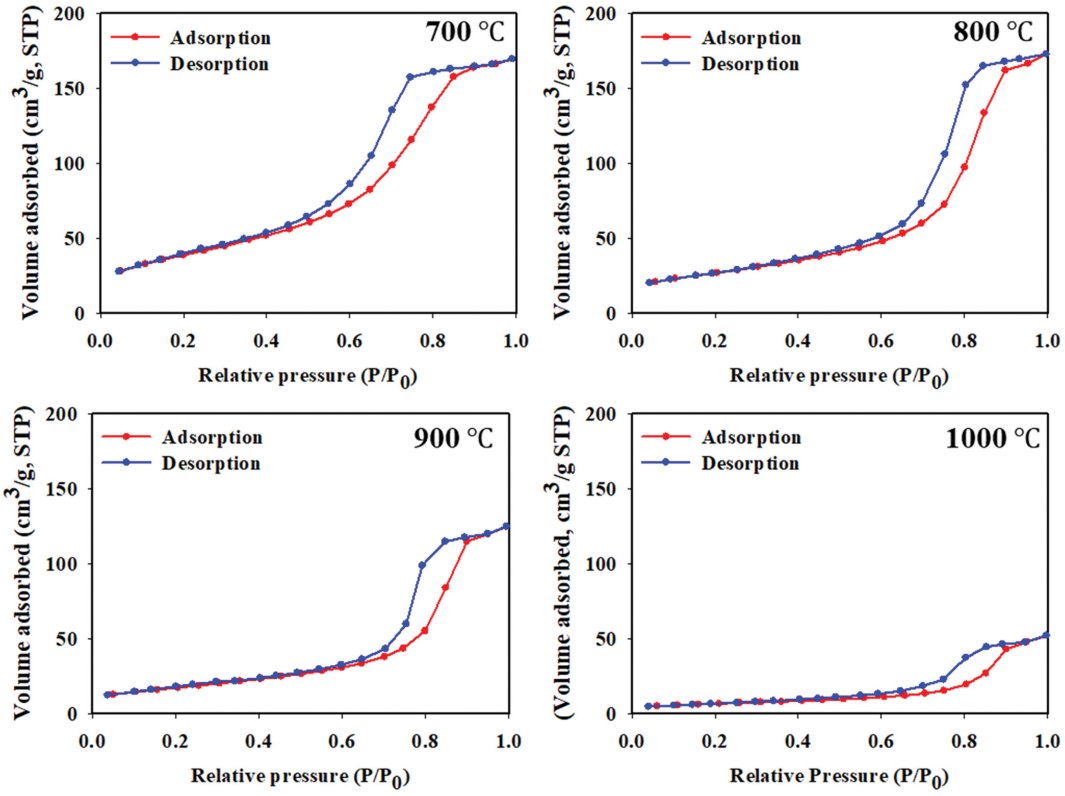

Fig. 8. N_2 adsorption-desorption isotherms of Ni(40)Mg(3)Al(57) calcined from 700 to 1,000 °C.

Table 2. Textural properties of Ni(40)Mg(3)Al(57) calcined at different temperatures

Calcination temperature (°C)	Surface area (m^2/g)	Total pore volume (mL/g)	Average pore size (Å)
700	140.2	0.2622	74.79
800	95.5	0.2673	111.9
900	62.4	0.1931	123.8
1,000	23.7	0.0805	136.0

ume also showed a similar tendency. As the calcination temperature increased, the position of hysteresis was shifted from the low P/P_0 to the high P/P_0, implying that small meso-sized pore collapsed and sintered, and thus, bigger pore was formed. Although the pore volume of the catalyst calcined at 1,000 °C was one-third of the catalyst calcined at 700 °C, the mean pore diameter was almost 1.8-times bigger.

Although the CO_2 hydrogenation was conducted in the fixed bed reactor (Fig. 2), the attrition resistance of the catalyst powders was measured to investigate their potential use for a fluidized bed reactor system. The results of attrition resistances are shown in Fig. 9 to quantify the particle strength. For all samples, the amount of wear loss during the initial 1 h was almost 80% of the total loss over 5 h of testing. This initial particle loss was probably due to the presence of small particles with low sphericity. Small-sized irregular powders were easily lost during the initial period, and thus, we compared particle loss during the 2nd to 5th hours using corrected attrition indices (CAI) which have been widely used [27]. CAIs of sample slightly increased as the calcination temperature increased.

As mentioned above, the crystallinity of Ni(40)Mg(3)Al(57) increased with calcination temperature but surface areas and pore volumes reduced. To investigate the effects of these physical properties on catalyst activity, CO_2 hydrogenation was carried out using Ni(40)Mg(3)Al(57) catalysts calcined at different temperature. As shown in Fig. 10, CO_2 conversion decreased slightly on increasing calcination temperature, which we believe was caused by the formation of a spinel phase and the poor textural property of samples calcined at higher temperature. Although particle strengths

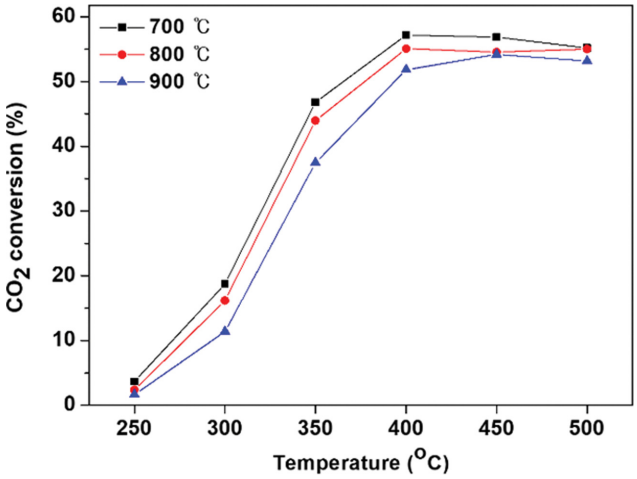

Fig. 10. CO_2 conversion by Ni(40)Mg(3)Al(57) calcined at different temperatures (GHSV=~20,000 h^{-1}).

Table 3. CO_2 conversion over prepared catalysts with different nickel loading and calcination temperature

Catalysts	Calc. Temp., °C	GHSV (h^{-1})	CO_2 conversion at 450 °C
Ni(20)Mg(3)Al(77)	700	30,000	6.1
Ni(30)Mg(3)Al(67)	700	30,000	39.7
Ni(40)Mg(3)Al(57)	700	30,000	44.1
Ni(60)Mg(3)Al(37)	700	30,000	50.3
Ni(40)Mg(3)Al(57)	700	20,000	56.9
Ni(40)Mg(3)Al(57)	800	20,000	54.5
Ni(40)Mg(3)Al(57)	900	20,000	54.2

were enhanced slightly on increasing calcination temperature, catalytic activity was decreased. If the catalysts were used for fluidized bed reactor, the particle strength would be considered as a priority. If not, the catalytic activity was generally a more important variable than the particle strength.

To compare the catalytic activity obtained by changing experi-

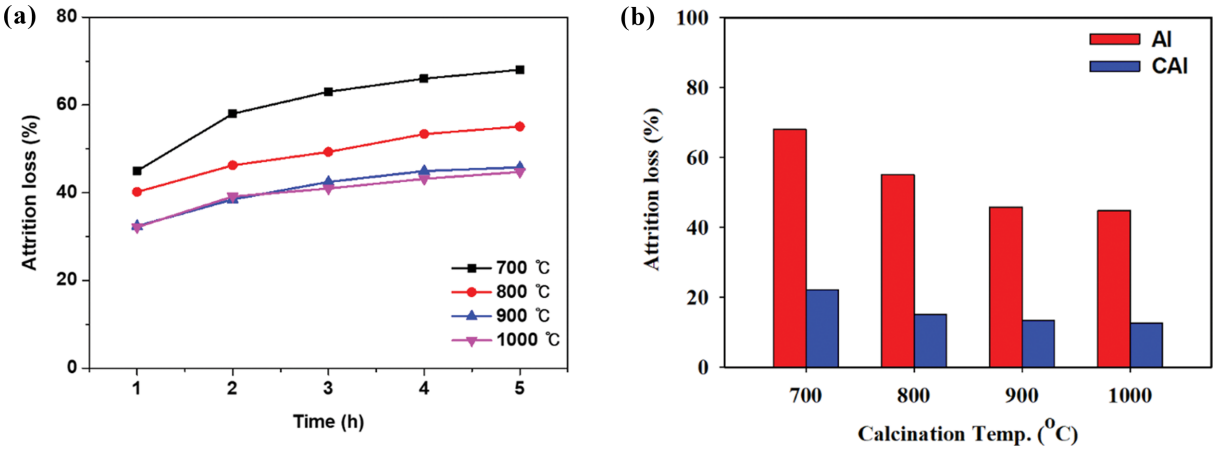

Fig. 9. Attrition resistance of Ni(40)Mg(3)Al(57) produced at calcination temperature from 700 to 1,000 °C; (a) attrition loss versus test time, and (b) attrition indices (AI) and corrected attrition indices (CAI) for catalysts prepared at different calcination temperatures.

mental parameters, CO_2 conversion of various samples is summarized in Table 3. The increase of CO_2 conversion with the increased nickel loading (Fig. 3) and decreased calcination temperature (Fig. 10) is clearly observed.

3. Catalytic Activity of Reduced $NiAl_2O_4$ and $MgAl_2O_4$ Spinel Oxides

As observed in Fig. 4 and 5, Ni (the main active species in CO_2 hydrogenation catalysts) forms a composite metal oxide with Al_2O_3 with a spinel structure, which reduces catalytic activity. In particular, the crystallinity of the $NiAl_2O_4$ spinel structure was further increased when calcination was performed at higher temperature to enhance wear resistance. To suppress $NiAl_2O_4$ formation, a MgO promoter was added to form $MgAl_2O_4$ spinel instead of $NiAl_2O_4$.

To investigate the effect of spinel phase formation in $NiAl_2O_4$ and $MgAl_2O_4$ on catalytic activity, spinel structures were synthesized by coprecipitation using nickel-alumina and magnesium-alumina combinations. The manufacturing process was carried out using the same procedure as that for coprecipitation described above, and Ni/Al and Mg/Al ratios in precursors were set at the stoichiometric ratio (AB_2O_4) of spinel structures. The catalysts produced were heat-treated at 1,000 °C to promote spinel formation. Subsequently, spinel structures were pretreated with H_2 and CO_2 hydrogenation was conducted using two spinel catalysts: $NiAl_2O_4$ and $MgAl_2O_4$.

CO_2 conversion using reduced $NiAl_2O_4$ and $MgAl_2O_4$ tended to increase with reaction temperature (Fig. 11(a)), which confirmed that reduced spinel structure can catalyze CO_2 hydrogenation. The high catalytic activity of the reduced $NiAl_2O_4$ was possibly due to the presence of metallic Ni generated during catalyst reduction. That is, some spinel structures could be reduced and the reduced Ni appeared to have high catalytic activity. On the other hand, the reduced $MgAl_2O_4$ showed significantly less conversion than the reduced $NiAl_2O_4$.

Selectivity for CH_4 and CO obtained by CO_2 hydrogenation using the two spinel catalysts is shown in Fig. 11(b). CO selectivity of reduced $NiAl_2O_4$ was ~70%, whereas almost only CO was produced by $MgAl_2O_4$. A small amount of CO was also produced when the reduced $NiAl_2O_4$ spinel structure was used as a CO_2 hydrogenation catalyst. At reaction temperature from 350 to 500 °C, an inverse relation was observed between CH_4 and CO production. The amount of CH_4 produced tended to increase as the amount of CO production decreased.

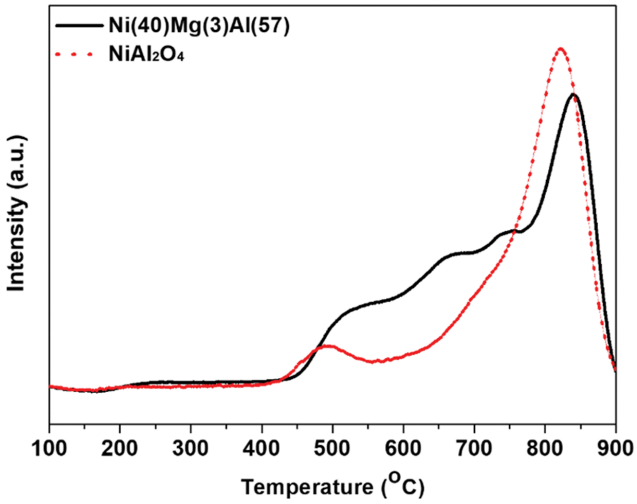

Fig. 12. H_2-TPR of $NiAl_2O_4$ and Ni(40)Mg(3)Al(57).

During CO_2 hydrogenation to CH_4 using a Ni-based catalyst, CO_2 is dissociated to form CO and the CO is further dissociated to surface adsorbed carbon [17,18], which combines with atomic hydrogen to produce CH_4 [28]. The reduced metal oxide composites $NiAl_2O_4$ and $MgAl_2O_4$ are considered to catalyze the dissociation of CO_2. The reduced $NiAl_2O_4$ was highly active for the CO_2 hydrogenation, but the reduced $MgAl_2O_4$ was less active. However, reduced $MgAl_2O_4$ may be non-catalytic in terms of the dissociation of surface-adsorbed CO. Therefore, CO was desorbed from reduced $MgAl_2O_4$, selectivity for CO was almost 100%, and CH_4 was not produced. On the other hand, reduced $NiAl_2O_4$ catalyzed the dissociation of surface-adsorbed CO, and CH_4 was produced with high selectivity, though a small amount of surface-adsorbed CO desorbed before dissociation to carbon.

The measured CO_2 hydrogenation activity of reduced $NiAl_2O_4$ and $MgAl_2O_4$, confirmed both catalyzed CO_2 hydrogenation but only $NiAl_2O_4$ catalyzed the dissociation of the surface-adsorbed CO. These results show excessive addition of MgO to Ni/Al_2O_3 catalyst detrimentally affects CO_2 methanation. On the other hand,

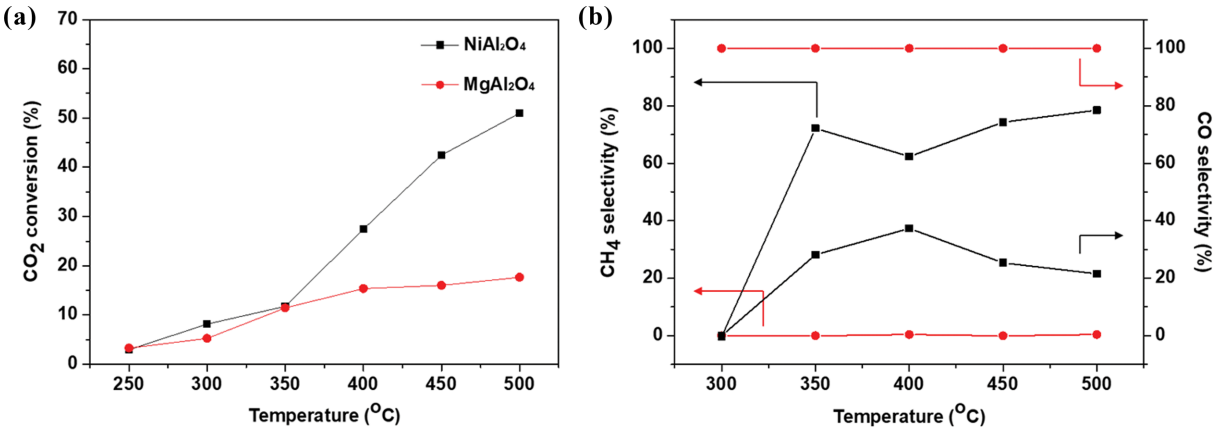

Fig. 11. CO_2 hydrogenation over $NiAl_2O_4$ or $MgAl_2O_4$ catalysts; (a) conversion of CO_2 and (b) selectivity for CO and CH_4 (GHSV=~20,000 h^{-1}).

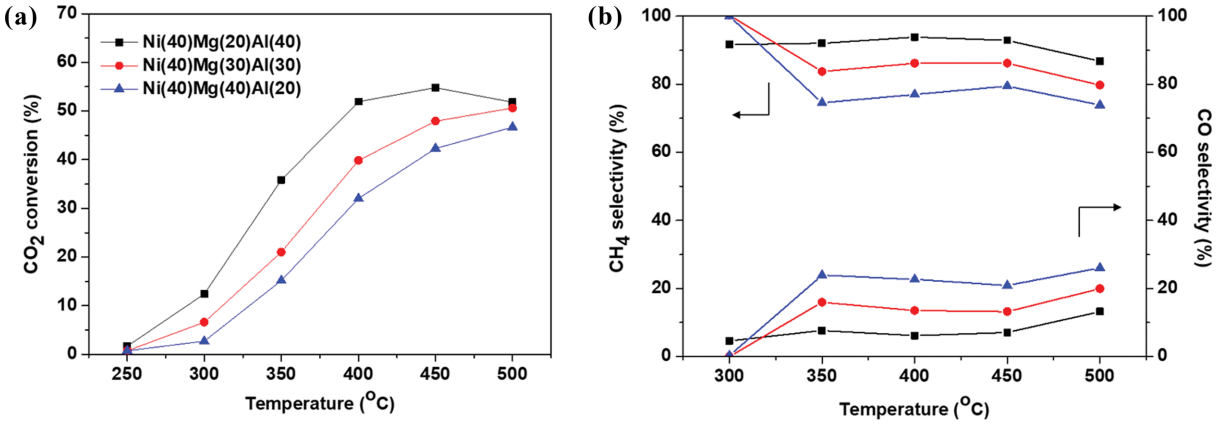

Fig. 13. Results for CO_2 hydrogenation over Ni-Mg-Al-based catalysts prepared at different Mg/Al mix ratios; (a) CO_2 conversion, (b) selectivity for CO and CH_4 (GHSV=~20,000 h^{-1}).

reduced $MgAl_2O_4$ could be used as a catalyst for RWGS because of its high CO selectivity.

To investigate the effect of the small amount of MgO addition on the reduction characteristic of the catalyst, H_2-TPR of $NiAl_2O_4$ was compared with that of Ni(40)Mg(3)Al(57) in Fig. 12. Reduction of oxide phases was much more easily carried out for the Ni(40)Mg(3)Al(57) catalyst than the $NiAl_2O_4$ catalyst, possibly due to the formation of $MgAl_2O_4$ rather than $NiAl_2O_4$.

To confirm the mechanism responsible for CO_2 hydrogenation by reduced $MgAl_2O_4$, an excessive amount of MgO was added to Ni-Al catalyst. NiO concentration was fixed at 40 wt% and different weight ratios of MgO to Al_2O_3 were used (20/40, 30/30, or 40/20). After coprecipitation, samples were aged for 12 h and then calcined at 1,000 °C for 4 h. The catalytic activity of the prepared samples is shown in Fig. 13. CO_2 conversion decreased on increasing the amount of MgO in the MgO-added Ni-Al catalyst (Fig. 13(a)). While the CH_4 selectivity of Ni(40)Mg(20)Al(40) was about 90% from 300 to 500 °C, that of Ni(40)Mg(30)Al(30) and Ni(40)Mg(40)Al(20) was lower at 85 to 70%, respectively, which confirmed the negative effect of MgO concentration on CH_4 selectivity.

When product yields were compared at a reaction temperature of 450 °C, decreases and increases in the yields of CH_4 and CO caused by adding MgO were more clearly observed (Fig. 14). CH_4 yield decreased from 50 to 35% when MgO concentration was increased from 20 to 40%, while CO yield increased from 5 to 10%.

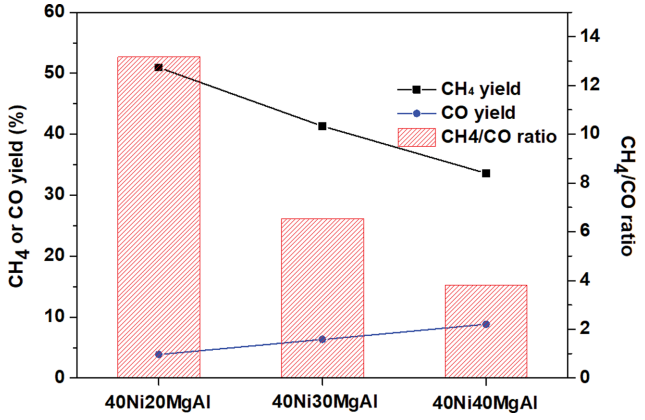

Fig. 14. Yield of CH_4 and CO, and CH_4/CO ratios for CO_2 hydrogenation conducted at 450 °C over Ni-Mg-Al- catalysts with different Mg/Al ratios (GHSV=~20,000 h^{-1}).

CONCLUSIONS

We investigated the catalytic activity of Ni-Mg-Al mixed oxide catalysts for CO_2 hydrogenation. The results obtained confirmed that higher NiO concentration in catalysts increased CO_2 conversion. When NiO concentration in NiO/Al_2O_3 was relatively low (20 wt%), $NiAl_2O_4$ was predominantly formed. Furthermore, a decrease in NiO, which produces catalytic sites after H_2 reaction, reduced CO_2 conversion.

Although elevated calcination temperature slightly increased particle strength, as measured by attrition testing, catalytic activity obviously decreased, presumably because higher calcination temperature enhanced the interaction between NiO and Al_2O_3, causing spinel formation, and decreased catalyst active surface area and pore volume.

MgO was used as an additive to suppress the high-temperature sintering of NiO and Al_2O_3. However, when MgO was added, the $MgAl_2O_4$ spinel structure was formed rather than $NiAl_2O_4$. Two spinel structures were reduced and tested for CO_2 hydrogenation. While the reduced $NiAl_2O_4$ showed high CH_4 selectivity, only CO was produced by reduced $MgAl_2O_4$. These observations show reduced $MgAl_2O_4$ can catalyze the dissociation of CO_2, but not the dissociation of surface-adsorbed CO. On the other hand, the dissociation of CO_2 to C was nearly complete on the surface of reduced $NiAl_2O_4$, and thus, CH_4 was produced from CO_2. To confirm the proposed reaction mechanism, more than 20% by wt of MgO was added to the catalyst, and as was expected as MgO concentration increased, CO_2 conversion decreased, and selectivity for CO increased due to the formation of $MgAl_2O_4$.

To achieve CO_2 hydrogenation to CH_4, it is important to use Ni-based catalysts and to prevent the formation of the $NiAl_2O_4$ spinel structure. To do this, MgO can be added, as the present study shows the formation of $MgAl_2O_4$ can increase CO selectivity during the hydrogenation of CO_2. Therefore, the amount of MgO added to

catalyst should be optimized to minimize the formation of $NiAl_2O_4$ and maximize selectivity for CH_4.

ACKNOWLEDGEMENTS

This work was conducted under framework of the research and development program of the Korea Institute of Energy Research (B9-2446). This work was supported by the 2019 Yeungnam University Research Grant.

REFERENCES

1. J. M. Guerrero, F. Blaabjerg, T. Zhelev, K. Hemmes, E. Monmasson, S. Jemeï, M. P. Comech, R. N. Granadino and J. L. Frau, *IEEE Ind. Electron. Mag.*, **4**(1), 52 (2010).
2. I. Dincer, *Renew. Sust. Energy Rev.*, **4**(2), 157 (2000).
3. R. W. J. Edwards and M. A. Celia, *PNAS*, **115**(38), E8815 (2018).
4. A. Al-Mamoori, A. Krishnamurthy, A. A. Rownaghi and F. Rezaei, *Energy Technol.*, **5**, 834 (2017).
5. J. D. Figueroa, T. Fout, S. Plasynski, H. Mcllvried and R. D. Srivastava, *Int. J. Greenhouse Gas Control*, **2**(1), 9 (2008).
6. D. Schack, L. Rihko-Struckmann and K. Sundmacher, *Ind. Eng. Chem. Res.*, **57**, 9889 (2018).
7. J. P. Barton and D. G. Infield, *EEE Trans. Energy Convers*, **19**(2), 441 (2004).
8. M. A. Ancona, G. Antonioni, L. Branchini, A. De Pascale, F. Melino, V. Orlandini, V. Antonucci and M. Ferraro, *Energy Procedia*, **101**, 854 (2016).
9. B. Lee, H. Lee, S. Kang and H. Lim, *J. Energy Storage*, **24**, 100791 (2019).
10. G. Zhou, H. Liu, Y. Xing, S. Xu, H. Xie and K. Xiong, *J. CO_2 Utilization*, **26**, 221 (2018).
11. M. Li, H. Amari and A. C. van Veen, *Appl. Catal. B: Environ.*, **239**, 27 (2018).
12. Y. Zhang, G. Jacobs, D. E. Sparks, M. E. Dry and B. H. Davis, *Catal. Today*, **71**, 411 (2002).
13. J. Wang, Z. You, Q. Zhang, W. Deng and Y. Wang, *Catal. Today*, **215**, 186 (2013).
14. M. Götz, J. Lefebvre, F. Mörs, A. M. Koch, F. Graf, S. Bajohr, R. Reimert and T. Kolb, *Renewable Energy*, **85**, 1371 (2016).
15. H. C. Wu, Y. C. Chang, J. H. Wu, J. H. Lin, I. K. Lin and C. S. Chen, *Catal. Sci. Technol.*, **5**, 4154 (2015).
16. K. Stangeland, D. Kalai, H. Li and Z. Yu, *Energy Procedia*, **105**, 2022 (2017).
17. G. D. Weatherbee and C. H. Bartholomew, *J. Catal.*, **77**(2), 460 (1982).
18. J. Y. Lim, J. McGregor, A. J. Sederman and J. S. Dennis, *Chem. Eng. Sci.*, **141**, 28 (2016).
19. K. B. Kester, E. Zagli and J. L. Falconer, *Appl. Catal.*, **22**, 311 (1986).
20. A. E. Aksoylu and Z. I. Onsan, *Appl. Catal. A*, **164**(1-2), 1 (1997).
21. S.-H. Kang, J.-H. Ryu, J.-H. Kim, S.-J. Seo, Y.-D. Yoo, P. S. S. Prasad, H.-J. Lim and C.-D. Byun, *Korean J. Chem. Eng.*, **28**(12), 2282 (2011).
22. G. Garbarino, P. Riani, L. Magistri and G. Busca, *RSC Adv.*, **5**, 22759 (2015).
23. J. Lin, C. Ma, Q. Wang, Y. Xu, G. Ma, J. Wang, H. Wang, C. Dong, C. Zhang and M. Ding, *Appl. Catal., B*, **243**, 162 (2019).
24. S. Rahmani, M. Rezaei and F. Meshkani, *J. Ind. Eng. Chem.*, **20**, 1346 (2014).
25. F. Meshkani, M. Rezaei and M. Andache, *J. Ind. Eng. Chem.*, **20**, 1251 (2014).
26. J. Bremer and K. Sundmacher, *React. Chem. Eng.*, **4**, 1019 (2019).
27. J. B. Lee, C. K. Ryu, J.-I. Baek, J. H. Lee, T. H Eom and S. H. Kim, *Ind. Eng. Chem. Res.*, **47**(13), 4465 (2008).
28. E. Vesselli, J. Schweicher, A. Bundhoo, A. Frennet and N. Kruse, *J. Phys. Chem. C*, **115**, 1255 (2011).